

Article

Ruby from Longido, Tanzania: Mining, Color, Inclusion, and Chemical Features

Yujie Gao ¹, Mingyue He ^{2,*}, Andrew Christopher Lucas ³, Xueying Sun ¹, Dan Zhou ³, Tiantian Huang ¹, Kai Li ¹, Darwin Fortaleché ⁴, Moqing Lin ¹, Yuan Zhu ² and Xiaoting Jin ⁵

¹ Guild Gem Laboratories, Shenzhen 518020, China; peter.gao@guildgemlab.com (Y.G.); shirley.sun@guildgemlab.com (X.S.); candice.huang@guildgemlab.com (T.H.); likai@guildgemlab.com (K.L.); linmoqing@guildgemlab.com (M.L.)

² School of Gemology, China University of Geosciences, Beijing 100183, China; zhuyuan27@cugb.edu.cn

³ Guild Institute of Gemology, Shenzhen 518020, China; andrew.lucas@guildgemlab.com (A.C.L.); dan.zhou@guild1980.com (D.Z.)

⁴ Guild Gem Laboratories, Bangkok 10310, Thailand; darwin.fortaleche@guildgemlab.com

⁵ Guangdong Provincial Gem & Precious Metal Testing Center, Guangzhou 510080, China; jinxt_shel@163.com

* Correspondence: hemy@cugb.edu.cn

Abstract: This article reports on the recent mining and production status of ruby in Longido, Tanzania. Faceted-grade rubies and their matrix from Longido Area, Tanzania, were investigated by standard gemological testing, including FTIR, UV-VIS, Raman spectra, and LA-ICP-MS. Microscopic observations revealed dense needle-like and triangular inclusions, distinct growth lines, and color banding as typical inclusions. In agreement with the Raman results, the transmission FTIR spectrum confirmed the presence of aluminum hydroxide. The Raman spectra identified associated minerals and inclusions, including zoisite, parasites, feldspar within the matrix, rutile, and diasporite in the ruby host. The chemistry analysis revealed a high amount of Cr and relatively low iron as a good indicator of geographic origin.

Keywords: ruby; Longido; Tanzania; amphibole; zoisite; feldspar; fluorescence



Citation: Gao, Y.; He, M.; Lucas, A.C.; Sun, X.; Zhou, D.; Huang, T.; Li, K.; Fortaleché, D.; Lin, M.; Zhu, Y.; et al. Ruby from Longido, Tanzania: Mining, Color, Inclusion, and Chemical Features. *Crystals* **2024**, *14*, 383. <https://doi.org/10.3390/cryst14040383>

Academic Editor: Yuri N. Palyanov

Received: 20 February 2024

Revised: 26 March 2024

Accepted: 4 April 2024

Published: 19 April 2024



Copyright: © 2024 by the authors. Licensee MDPI, Basel, Switzerland. This article is an open access article distributed under the terms and conditions of the Creative Commons Attribution (CC BY) license (<https://creativecommons.org/licenses/by/4.0/>).

1. Introduction

Rubies are the red variety of corundum, bearing a very high reputation in the gem trade [1]. The color gemstone trade has benefited from global trade, new mining discoveries, and new markets. The gemological features of rubies are always fascinating to dealers and gem collectors. As rubies can be found worldwide, their gemological features and the mining situation can vary from one place to another. Three commonly encountered rock matrices contain commercial-quality ruby, i.e., marble, basalt, and amphibolite (Table 1).

The rubies formed in marble along the Himalayan Mountain belt are found in both the primary and placer deposits [2,3]. Mogok in Burma (“Burma” is the former name of the state now officially called “Myanmar”) is reputed for producing high-quality rubies for centuries [4–6], and some of the Mong Hsu rubies were also formed in marble [7]. While the rubies found in Vietnam also show good quality [8–10]. Previous studies also reported rubies from Ailao Shan in Yunnan Province, China [11,12]. Due to their richness in Cr and lack of Fe, the marble-hosted rubies usually exhibit a bright hue and strong red fluorescence.

Alkali basalt rocks are reported to contain ruby and sapphire, where the erupting magma captures the ruby and sapphire formed in the upper mantle as xenocrysts within the basalt. The formation model of gem corundum from alkali basalt has been proposed by previous studies [13,14]. Ruby and sapphire associated with basalt are found in Thailand/Cambodia, New South Wales, Australia, and Montana, USA [15–18].

Table 1. Three commonly encountered rock matrices and their representative sources.

Rock Matrices	Source
Marble	Burma (Mogok/Mong Hsu)
	Vietnam
Amphibolite	China (Ailao Shan, Yunnan Province)
	Mozambique
	Madagascar
	Tanzania
Basalt-related	Thailand/Cambodia
	New South Wales
	Australia
	Montana, USA

Amphibolite-hosted ruby can be found in Africa, including Mozambique, Madagascar, and Tanzania [19–24]. Greenland is also reported to produce ruby in the amphibolite hard rock [25–28].

Ruby from Burma may command a premium on price owing to its long history and high quality [2,29,30]. It is critical to document the information in the field and the characteristics of the ruby to disclose the essential information to the public fully and, as a result, increase their confidence.

Tanzania has been known for producing various gems for decades [31], such as rubies from Winza and Longido [32,33], sapphires from Umba Valley [34], spinels from Mahenge [35,36], tsavorite garnet [37,38], alexandrite [39], and tanzanite. Cabochon-quality rubies have been discovered in the Longido area for over half a century. Recently, faceted-quality materials have been produced in Longido, causing a fever in the gem market in a short time. Previous studies reported the gemological features of the ruby from Longido, Tanzania [40–43].

The authors of this research provide first-hand knowledge of the mining region. We use various testing techniques to examine the gemological characteristics of Longido rubies. To distinguish the origins, reveal more important information, and increase transparency, we also compare rubies from Longido, Mozambique, and Burma on a broad scale [43].

2. Geological Background

Geologically, Tanzania is situated on an Archean craton. This granitic center is surrounded by crystalline rocks that get younger and younger. At the same time, the rifted grabens, coastal plains, and interior basins are made up of Paleozoic to recent sediments and volcanics. According to Schlüter [44], there is a good representation of rocks from the Archean, Proterozoic, Paleozoic, Mesozoic, and Cenozoic eras. As previously indicated, the geological setting's variety gives rise to an abundance of gemstones.

Several ruby mines have been found in Tanzania, and their gemological features, such as Winza and Morogoro, were studied by previous literature [33,45]. The Longido area lies near the border between Tanzania and Kenya, as indicated in Figure 1. Ruby was discovered in Longido, Tanzania, in 1949 by two English prospectors who lived in Nairobi, Kenya, searching for minerals and gems in the African wilderness. After weeks of exhausting searching in this area, one of the prospectors named Tom Blevins came to an outcrop of weathered green rock and noticed well-formed flat tabular and hexagonal-shaped deep red ruby crystals laying on the rock. The smaller ones had transparent areas and were facet grade, while larger ones still in the green rock were opaque but with their distinctive hexagonal shape and red color, making a striking appearance against the green host rock they were in. However, earlier accounts of rubies are found in Longido, dating back a hundred years. Mining was conducted in the late 1950s.



Figure 1. The illustration of ruby mine distribution in Tanzania. Illustrated by Huixin Zhao.

Large amounts of material were initially found near the surface, but now most mining requires extensive tunneling. Most Longido rubies are found in green zoisite and dark amphibolite rocks. Most are nearly opaque and used for beautiful carving material. In fact, ruby in green zoisite can make an amazingly beautiful and striking carving material, which skilled carvers can make into carvings where the two opposite colors complement each other. While only a small portion of the production meets the criteria for transparent facet grade, these rubies can display a stunning “Pigeon’s Blood” red color if they were cut in half and three-quarter carat-size faceted stones without requiring heat treatment. However, it is worth noting that rubies over one carat may appear overly dark.

3. Mining and Production

Large quantities of Longido small “Pigeon’s Blood” red unheated facet-grade ruby rough entered the Chinese market through Nairobi, Kenya, in late 2017 and early 2018. This new excitement led Guild to travel to Longido, Tanzania, with Chinese and local contacts to document the mining activity and material being mined just before the 2018 September Hong Kong Show (Figure 2a–c).

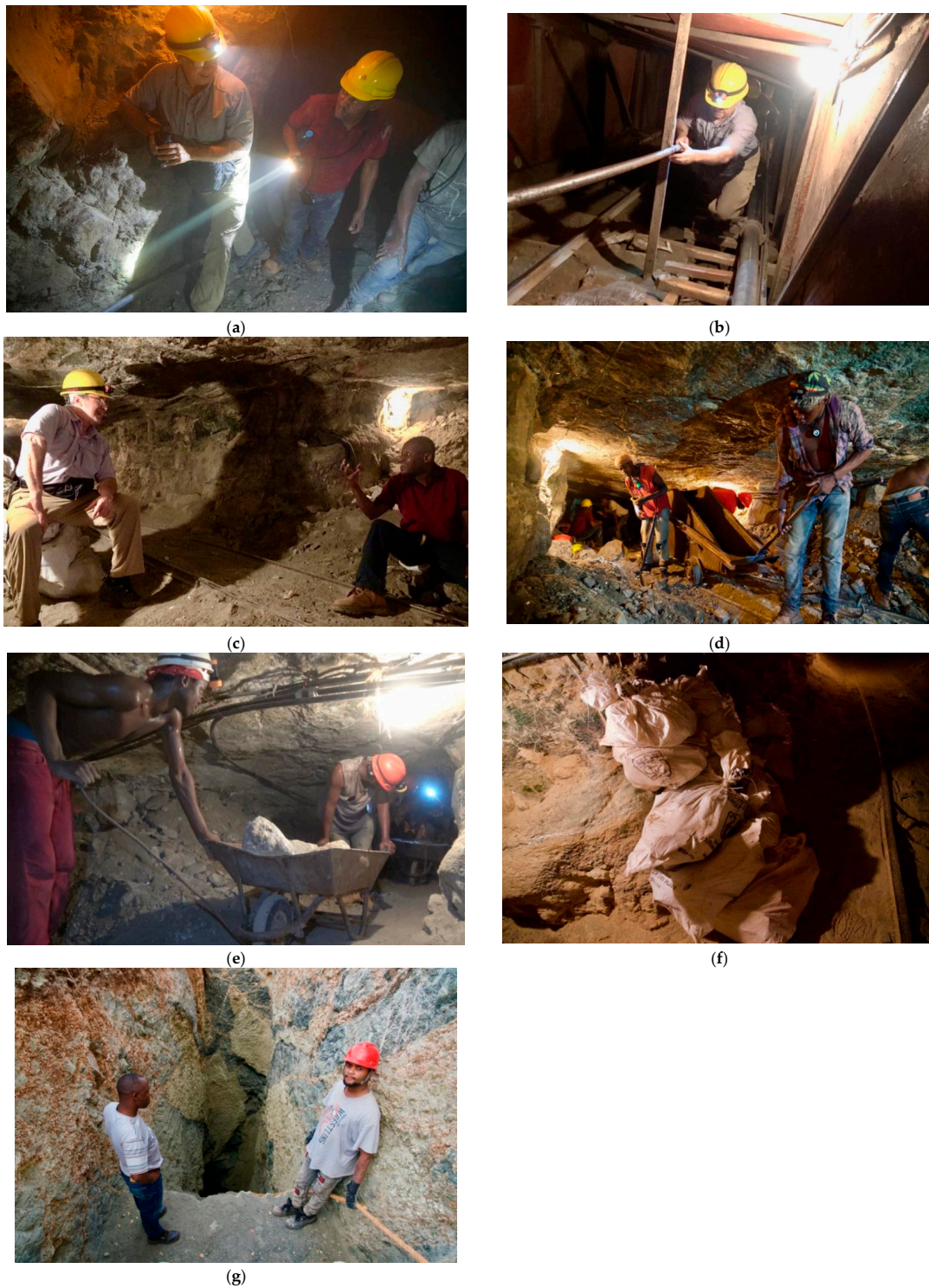


Figure 2. (a) In 2018, Guild Field Gemology Team documented ruby mining activity in Longido, Tanzania. (b) Author Andrew Lucas expressed that getting down to the productive mining zone elevations and backing up in the tunnels was a strenuous activity. (c) The mine manager gave a detailed account of the recent mining activity while in the tunnel. (d) The ruby mine tunnels can require miners to work bent over while mining the hard rock. (e) Human muscle power and endurance are primarily the forces required to mine in the hard rock ruby mine tunnels of Longido. (f) Bags of valuable facet-grade ruby rough are sealed and left deep in the mine for security. (g) This tunnel was less than three months old. Ruby has yet to be found. Photos copyright of Guild Institute of Gemology.

The tunnel mine that Guild Field gemologist Andrew Lucas documented had a long mining history and extended for hundreds of meters. After arriving in Arusha, we drove to Longido. Africa is such a fantastic place to visit, especially Tanzania. While going to Longido, we had to stop several times for wild animals to cross. During the visit, Andrew Lucas interviewed the mine manager about mining in 2017 and 2018. According to him, a large pocket of tiny and fine-color transparent crystals was discovered in 2017. This led to large purchases by Chinese buyers and much larger mining activity. In fact, the area near the mine changed from a few huts to over 1000 homes. Foreign investment also came into the mine to increase the mining pace and hopefully find more pockets of this quality material.

Mining work is very strenuous. This is the process of mining hard rock tunnels (Figure 2d–f). Once a pocket is reached, drills and jackhammers are used to remove the ruby, along with some hand tools. It is difficult to move the tunnel forward through the hard rock. The larger you make the tunnel, the more time, labor, and expense are involved, so in some areas, miners have to work bent over while digging in the hard rock. Gases released from the earth in the tunnel mixed with the fumes from the power tools and dust in the air, making ventilation at the deeper depths difficult. Two strong miners in their twenties had to be evacuated due to the fumes while Andrew Lucas was documenting in the tunnel.

While in the area, Andrew Lucas also visited recently developed ruby mines. The tunnels were still relatively shallow, and they were still just exploring for ruby. Some were less than a hundred meters deep (Figure 2g). The valuable pockets found in 2017 increased interest and investment in prospecting for the next tunnel that contained the yet-undiscovered pocket that would make the miners rich.

4. Materials and Methods

In this study, we used various techniques to characterize both the ruby and its matrix. Four large wall rocks were selected, and slices were cut and polished from them to analyze the associated minerals (Figures 3 and 4). A parcel of ruby rough was also investigated; however, because the surface of the rubies was coarse and unpolished, the internal features could not be studied. In addition, 39 pieces of faceted rubies were also studied (Figure 5); the majority of the rubies are highly saturated with bright to deep red tones, weighing from 0.50 ct to 1.00 ct in rough and 0.25 to 1.07 ct in faceted stones.

Refractive indices and birefringence were examined using a reflectometer and a light source with a near-sodium equivalency at Guild Gem Laboratories. The hydrostatic technique was used to calculate and determine the specific gravity. A portable dichroscope was utilized to observe pleochroism. In a dark environment, fluorescence responses were seen while exposed to conventional long-wave (365 nm) and short-wave (254 nm) U.V. light. To explore the interior characteristics, we used a typical geological microscope with Leica lenses and a magnification of up to 80 \times .

The infrared spectra of rubies were tested by a TENSOR II type Fourier transform infrared spectrometer (FTIR) from the German Bruker Optics company (Ettlingen, Germany) at Guild Gem Laboratories (Shenzhen, China) at room temperature (23 °C). The light source was near-infrared (NIR), with a scan range of 4000–1500 cm^{-1} , a resolution of 4 cm^{-1} , and a scan frequency of 3.75 kHz. Ninety-three ruby spectra, including 39 faceted and 54 rough samples, were collected for this investigation.

In this study, we have applied two main testing techniques EDXRF (Energy-Dispersive X-ray Fluorescence) and LA-ICP-MS (Laser Ablation Inductively Coupled Plasma Mass Spectrometer) to analyze the trace elements of rubies from Longido, Tanzania. These two techniques bear both advantages and disadvantages. For example, while EDXRF is very quick and simple to use on gemstone samples, it can only detect a limited number of elements. Light elements, such as Be, Li, and Na et al., are beyond the detection range. However, this method is non-destructive, which makes it possible to perform routine testing during daily testing in a gem lab. By comparison, it usually takes a professional expert to practice testing using LA-ICP-MS [46]. This method could detect most elements,

including light elements, at a higher accuracy level. But the laser applied by this method would cause a certain amount of destruction and leave a small hole in the sample. Such a method is destructive, and it should be very carefully operated.

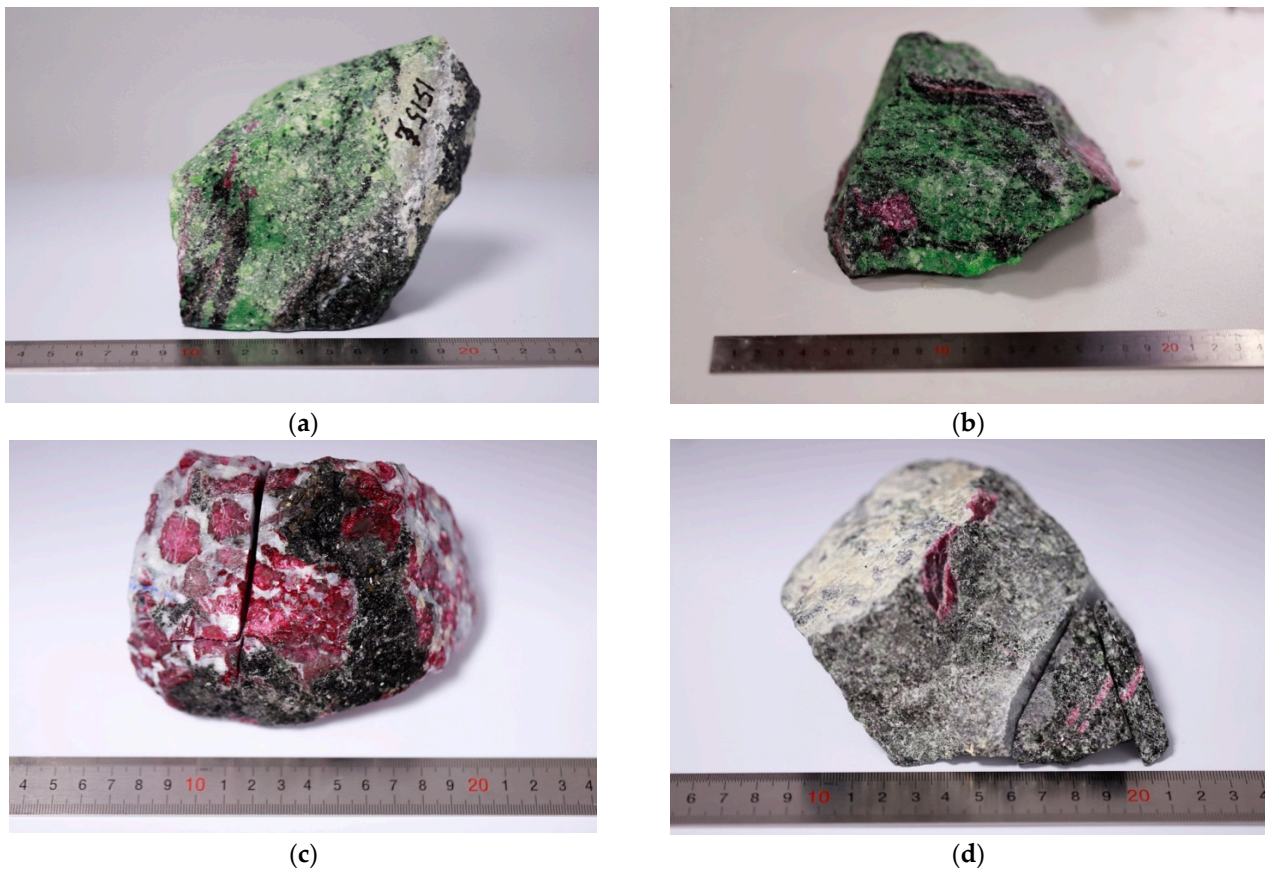


Figure 3. Rubies within the matrix are associated with green zoisite (a,b), deep green amphibole (a,b), and white feldspar (c,d). Photos by Yizhi Zhao.

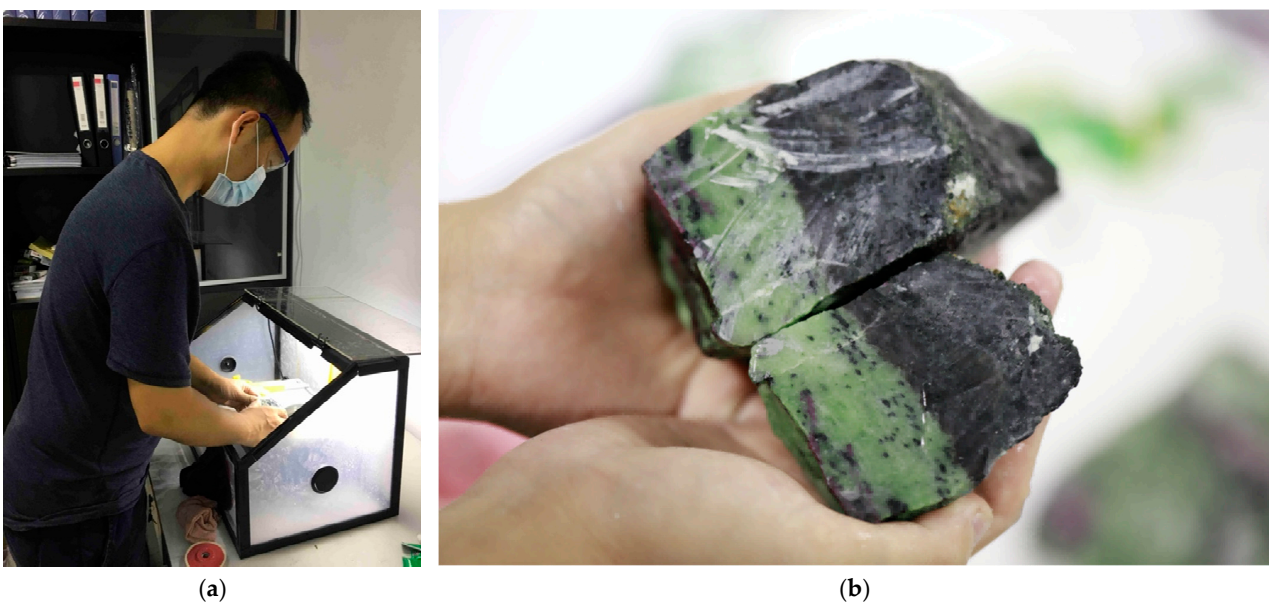


Figure 4. The wall rock specimen was cut into two parts by author Yujie Gao (a), showing the fresh face and distinct color distribution (b). Photos by Yizhi Zhao.



Figure 5. In this study, 39 pieces of faceted ruby from Longido, Tanzania, weigh 0.25 to 1.07 ct. Photo by Yizhi Zhao.

At the Wuhan Sample Solution Analytical Technology Co., Ltd., in Wuhan, China, the chemical compositions of associated minerals and the rubies were examined using laser ablation inductively coupled plasma mass spectrometry (LA-ICP-MS). A 193 nm ArF excimer laser ablation system (GeoLasPro) connected to an Agilent 7700 ICP-MS (Santa Clara, CA, USA) was used for trace element analyses. The laser energy was set at 80 mJ, the laser frequency to 5 Hz, and the spot diameter at 44 μm . The carrier gas was helium. The core gas flow of the Ar plasma (Ar + He) was supplemented with nitrogen to increase the detection limit and accuracy [47]. The USGS standards (BCR-2G, BHVO-2G, and BIR-1G) were utilized as an external standard, and NIST610 was examined for time-drift correction every six analyses. ICPMSDataCal conducted time-drift correction, time-selection, integration of background and analytical signals, and quantitative calibration for trace element analysis [48,49].

The chemical composition studies were also carried out at Guild Gem Lab utilizing a Ta target with a spot size of 2 mm and an energy-dispersive X-ray fluorescence (ED-XRF) device of the Spectro Midex type (Kleve, Germany) [50]. Al, Si, K, and Ca were tested using the RoHS+Bigspot technique at an acceleration voltage of 19 kV and a beam current of 0.30 mA, whereas Ti, V, Cr, Mn, Fe, Co, Ni, Cu, Ga, and other elements were tested at 48 kV and a beam current of 0.60 mA.

5. Results

5.1. Standard Gemological Analysis

In this study, the gemological characteristics of ruby from Longido were typical for corundum in general and similar to those of African rubies previously observed. Details on the gemological features of rubies in this study can be found in Table 2 below. The samples generally exhibit an intense and uniform red color of medium to high saturation, which is also called “Pigeon’s Blood” in the trade. Unlike the typical semi-transparent material from Longido, which is fashioned into carving, all the rubies are of very high transparency and gem-quality for faceted stones. The refractive index value is 1.762–1.770, with a birefringence of 0.008 and a specific gravity of 4.00, which is consistent with ruby from other locations. Most samples showed distinct strong fluorescence under long-wave UV light, and showed nearly inert to weak red under short-wave UV light.

Table 2. The gemological properties of ruby from Longido, Tanzania.

Property	Rubies in This Study
Color	red, medium to high saturation
Transparency	transparent
Quality	faceted quality
Pleochroism	red, purplish red
Refractive Index	$n_o = 1.762$, $n_e = 1.770$
Birefringence	0.008

Table 2. Cont.

Property	Rubies in This Study
Specific Gravity	4.00
Spectroscope	typical chromium spectrum, wide bands at about 410 nm to 555 nm from Cr ³⁺ ; luminescence line at 694 nm from Cr ³⁺
Fluorescence	L.W. (365 nm): strong red S.W. (265 nm): nearly inert to weak red
Chemical Fingerprint	high Cr concentration, relatively low Fe concentration
Internal features	twinning, color banding, needles, triangular platy, dark granular mineral, and diaspore

5.2. Wall Rock and Crystal Habit

From the perspective of crystal habit, the rough rubies examined in this study predominantly exhibit subhedral or anhedral shapes. Within the feldspar matrix, well-formed euhedral hexagonal crystals were seen. The majority of the crystal faces that were visible on the roughs were basal planes (0001), hexagonal prisms (10 $\bar{1}$ 0), and rhombohedra (11 $\bar{2}$ 1). And some well-formed crystals also existed with the crystal faces mentioned above, mainly with a platy shape owing to the excessive development of rhombohedra faces. Figures 6–11 depict ruby crystals embedded in the white feldspar, green to dark green zoisite, and dark-colored amphibole of the wall rocks. The related section on each mineral will go into further detail.

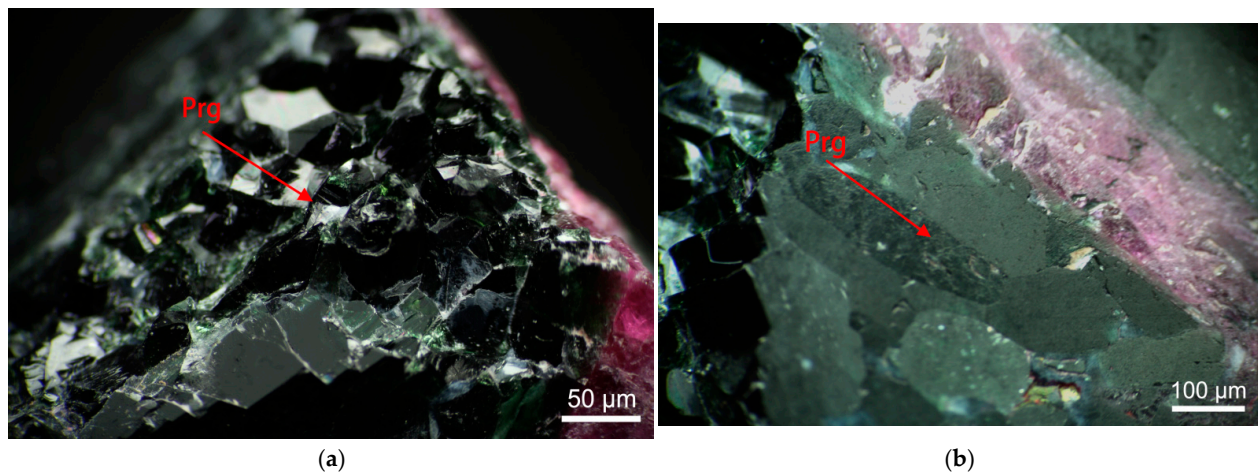


Figure 6. (a) Pargasite (Prg) of deep green body color exhibit sub-prismatic crystal habit. (b) The low tone of the body color may be attributed to the high content of iron. Photos by Yizhi Zhao.

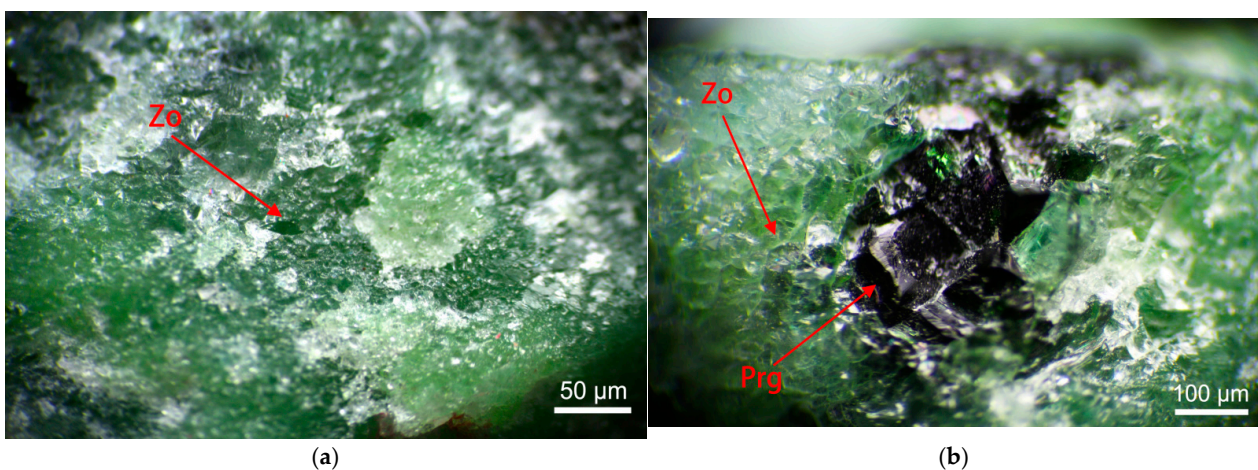


Figure 7. (a,b) Granular zoisite (Zo) minerals occur with deep green pargasite. Photos by Yizhi Zhao.

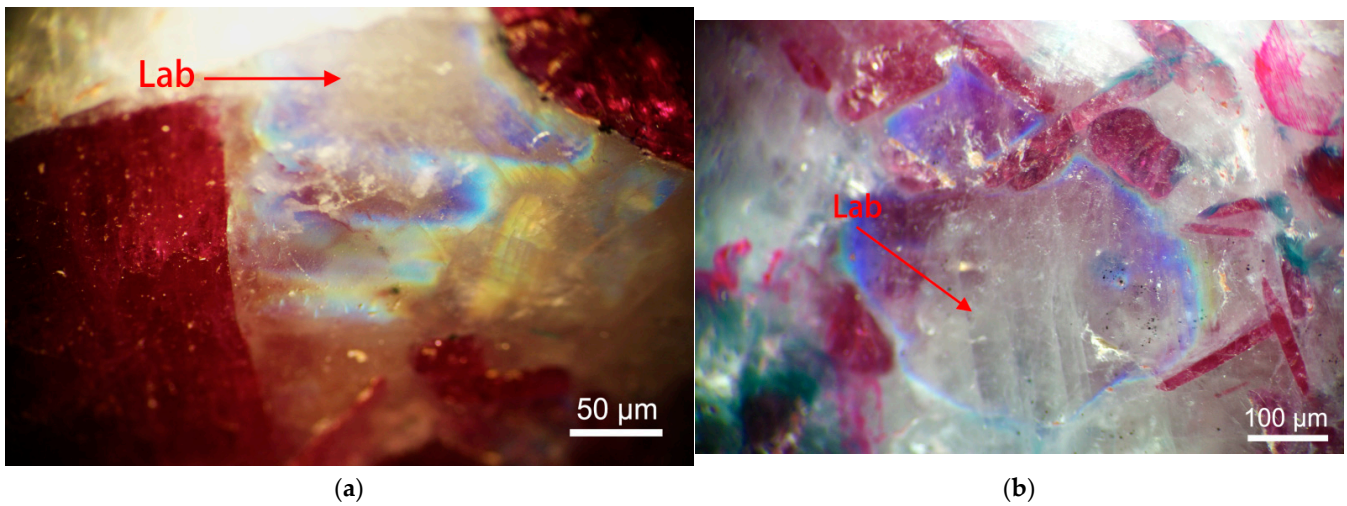


Figure 8. (a,b) Labradorite (Lab) minerals in the matrix. Photos by Yizhi Zhao.

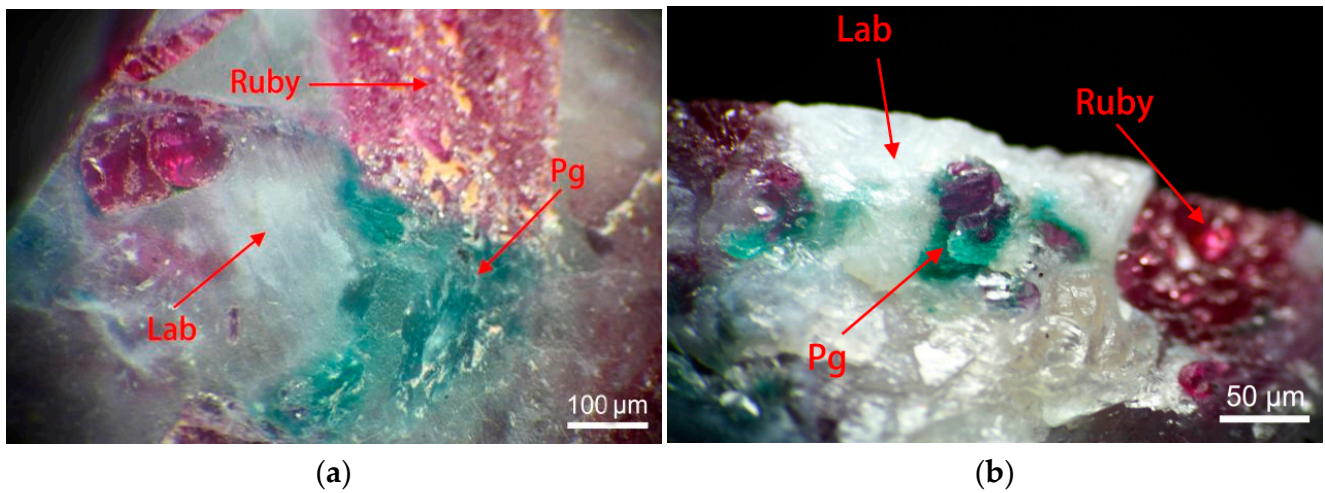


Figure 9. (a,b) Paragonite (Pg), with bright bluish-green color, always occurs by the rim of rubies and labradorite (Lab).

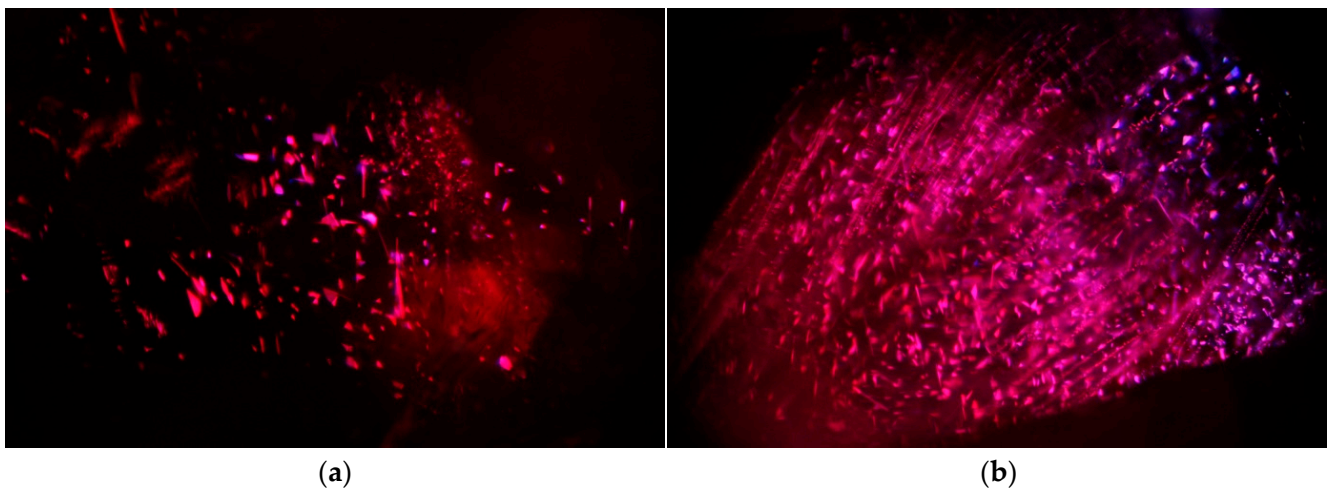


Figure 10. (a,b) Raman identified platy and short needle-like inclusions found in Longido rubies as rutile. Photomicrographs by Yizhi Zhao. Field of widths: (a) 3.25 mm and (b) 6.20 mm.

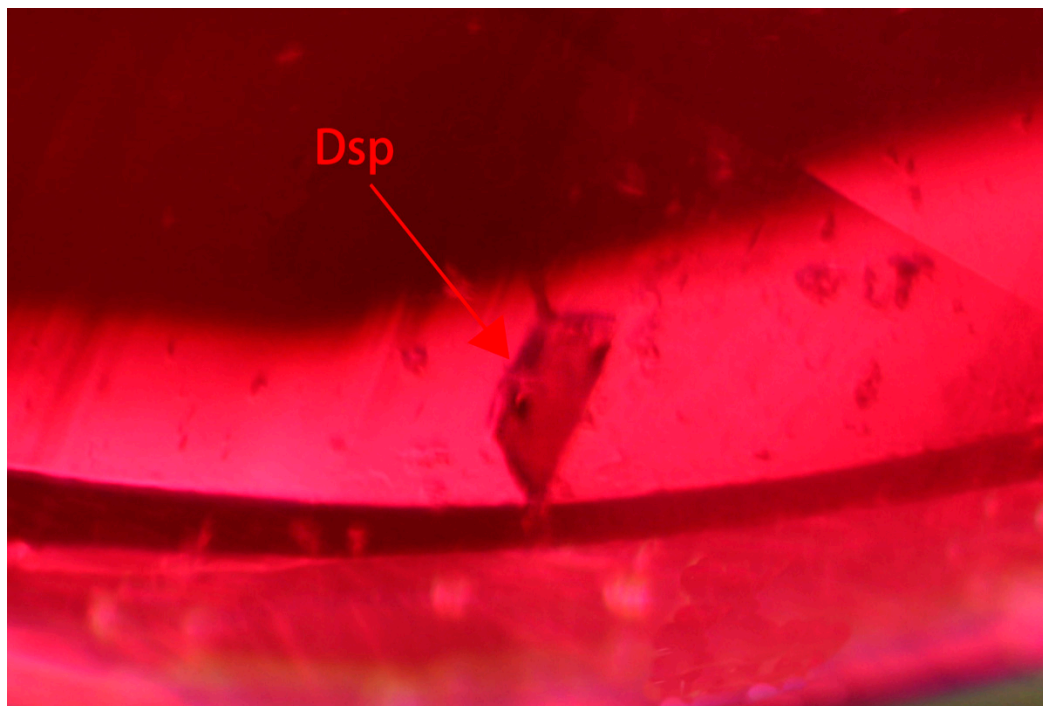


Figure 11. A transparent colorless crystal near the griddle of one ruby sample was confirmed as a diaspore (dsp) by Raman. Photomicrograph by Yizhi Zhao. Field of width: 4.10 mm.

5.3. Associated Minerals

Several associated minerals have been observed and identified, including pargasite, zoisite, labradorite, and paragonite. Their chemical composition results are listed in Table 3. The crystal-chemical formulas are calculated based on the data in Table 3 and listed in Table 4. All the minerals and crystal inclusions were identified by Raman spectra, as illustrated in Figures 12 and 13, with spectra from RRUFF as a reference (rruff.info).

Table 3. Chemical composition of corundum and associated minerals detected by LA-ICP-MS.

Oxides (wt%)	Corundum		Labradorite-Andesine		Pargasite	Zoisite
	Range (n = 11) ^a	Average	Range (n = 2) ^a	Average	(n = 1)	(n = 1)
BeO	bdl–0.04	0.01	—	—	—	0.0001
Na ₂ O	bdl–0.01	0.001	6.03–6.11 (6.07) ^b	6.07	3.27	0.001
MgO	0.002–0.063	0.01	0.0009–0.0010 (0.001)	0.001	14.69	0.05
Al ₂ O ₃	97.10–98.40	97.88	27.60–27.94 (27.77)	27.77	19.69	32.27
SiO ₂	0.85–1.57	1.11	55.62–55.91 (55.76)	55.76	41.46	40.57
P ₂ O ₅	bdl–0.25	0.06	0.11–0.15 (0.13)	0.13	0.06	—
K ₂ O	bdl–0.02	0.003	0.0535–0.0538 (0.0536)	0.0536	0.4	—
CaO	bdl–0.07	0.02	9.82–9.84 (9.83)	9.83	12.85	24.71
FeO	0.16–0.74	0.48	0.027–0.036 (0.032)	0.032	6.4	1.73
Total		99.574		99.6466	98.82	99.3311

^a n = number of measurements. ^b Minimum and maximum values are given, along with average; bdl = below detection limit.

Table 4. Ideal and calculated chemical composition of associated minerals in this study.

Associated Mineral	Ideal Chemical Compositions	Chemical Compositions in This Study
Pargasite	NaCa ₂ [(Mg,Fe) ₄ Al](Si ₆ Al ₂)O ₂₂ (OH) ₂	(Na _{0.85} K _{0.07} □ _{0.08})(Ca _{1.95} Na _{0.05})(Mg _{3.10} Fe _{0.75} Al _{0.15})Al _{1.00} (Si _{5.87} Al _{2.13})O ₂₂ (OH) ₂
Zoisite	Ca ₂ Al ₃ (SiO ₄)(Si ₂ O ₇)O(OH)	Ca ₂ (Fe _{0.41} Al _{2.59})(SiO ₄)(Si ₂ O ₇)O(OH)
Paragonite	NaAl ₂ (Si ₃ Al)O ₁₀ (OH) ₂	Not detected
Labradorite-Andesine	Na _{0.5-0.3} Ca _{0.5-0.7} Al _{1.5-1.7} Si _{2.5-2.3} O ₈	(Na _{0.53} Ca _{0.47})[Al _{1.47} Si _{2.53} O ₈]

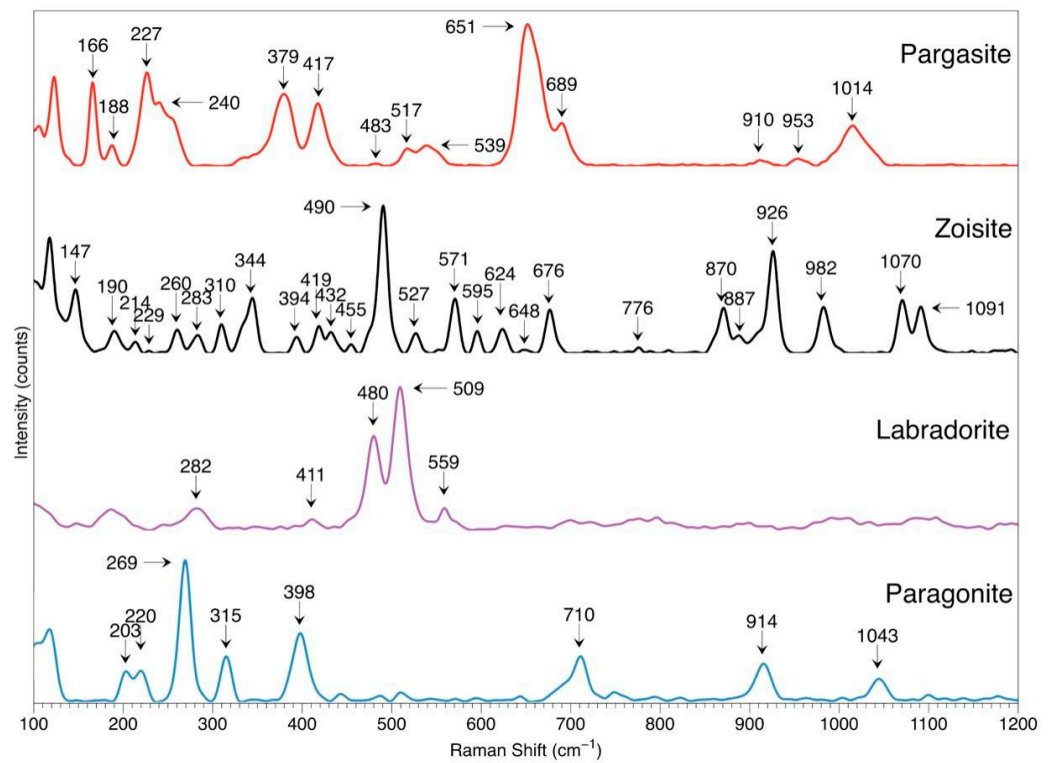


Figure 12. The Raman spectrum of four identified associated minerals from the ruby wall rock, including zoisite (black line), pargasite (red line), paragonite (blue line), and labradorite (purple line). Illustrated by Huixin Zhao.

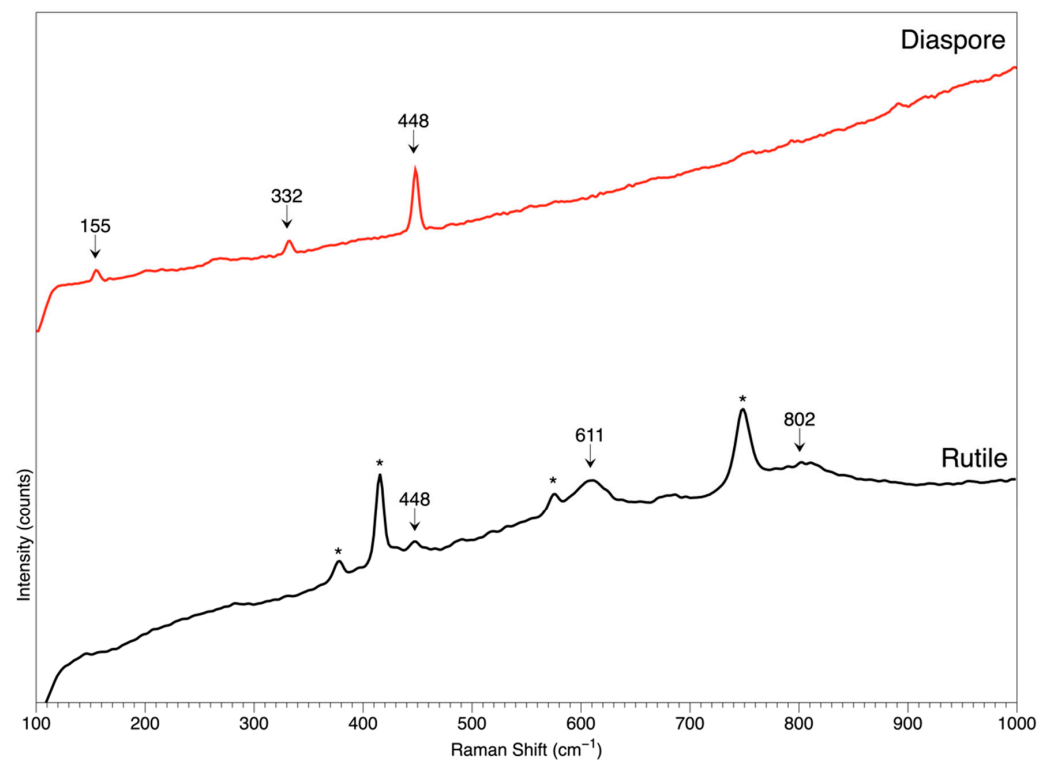


Figure 13. The Raman spectrum identifies the rutile (black line) and diaspore (red line) inclusions. Peaks in the inclusion spectra that are marked with * are from the host ruby. Illustrated by Huixin Zhao.

5.3.1. Pargasite Amphibole

The Raman spectra accurately identify the deep-colored crystal as pargasite, revealing characteristic peaks at 651, 227, 166, 379, and 417 cm^{-1} , which are consistent with those documented in the RRUFF database, as shown in Figure 6. Pargasite is an amphibole mineral with the ideal chemical formula $\text{NaCa}_2[(\text{Mg}; \text{Fe})_4\text{Al}](\text{Si}_6\text{Al}_2)\text{O}_{22}(\text{OH})_2$ (Table 4). As shown in Figure 8, the pargasite crystals within the matrix exhibit a deep green body color and sub-prismatic crystal habit. The dark tone of the body color may be attributed to the high iron content. The presence of pargasite is a good indicator that the Longido ruby formed in an amphibole-hosted deposit, which is similar to those found in Mozambique.

5.3.2. Zoisite

Zoisite is mainly formed together with pargasite as granular grains in the matrix, which is identified by the Raman spectra with characteristic peaks at 490 and 926 cm^{-1} (Figure 6). The previous production material was of cabochon quality, and ruby and zoisite compositions are usually fashioned as carvings to show ruby and green colors. So, it is not surprising to find zoisite with the new production ruby. Chemical analysis revealed that these green-associated minerals contain high levels of iron, up to 1.73% by weight, which may explain why the rubies contain less iron and exhibit a brighter color and stronger red fluorescence. Details can be found in Section 6.

5.3.3. Labradorite Feldspar

Ruby crystals were discovered near white minerals and some greenish-blue minerals. The Raman spectra identify these white minerals as labradorite, with peaks at 509 and 480 cm^{-1} , which is consistent with RRUFF.info. Labradorite is one member of the plagioclase series in the feldspar group. Labradorite exhibits distinct interference colors composed of blue and green when viewed under reflecting light. Furthermore, perfect cleavages were also observed, which agrees with the mineralogical property of labradorite (Figure 10).

5.3.4. Paragonite Mica

The green particles fit in the gap between ruby and labradorite, and they are identified as paragonite by Raman spectra, showing distinct peaks at 269, 398, and 315 cm^{-1} , consistent with that from RRUFF.info. Paragonite belongs to the mica group, with an ideal chemical composition of $\text{NaAl}_2(\text{Si}_3\text{Al})\text{O}_{10}(\text{OH})_2$. Paragonite is an uncommon mineral, and it could be found in large amounts, such as in low- to medium-grade metamorphic schists and phyllite, in muscovite-biotite gneisses, quartz veins, fine-grained sediments, and glaucophane-bearing rocks [51]. This study discovered paragonite minerals with a green color and silky luster within the feldspar matrix. It is very important to point out that all these green paragonites are only found in the reaction zoning between ruby and feldspar (Figure 11).

The source of Cr during the formation of ruby is still unclear. It is hypothesized that paragonite might have played a role in bringing Cr into the formation system of corundum, contributing to the red color. Further study is needed to decode the origin of Cr.

5.4. Associated Minerals and Inclusions

5.4.1. Rutile

As a common guest, rutile inclusions have been found in rubies from many locations, such as Burma, Mozambique, and Sri Lanka, as well as rubies from Longido, in this study. The Raman spectra confirmed the identity as rutile with feature peaks of 607 cm^{-1} (Figure 7). Rutile is an oxide mineral composed of Ti and O. Such mineral inclusions usually scatter in Longido ruby in the form of platy and short needles (Figure 12). The distinct visual appearance may facilitate the determination of the origin, which will be further explained in Section 6.

5.4.2. Diaspore

Diaspore is a hydro-aluminum oxide commonly seen in corundum. They are typically distributed on a submicroscopic scale and are inaccessible to the naked eye or even high magnification under microscopic examination. However, in this study, we discovered a transparent colorless subhedral crystal near the girdle of one faceted ruby sample (Figure 13), which is confirmed as a diaspore by Raman spectrum peaks at 448, 332, and 155 cm^{-1} , which agrees with RRUFF (Figure 6). Additionally, the FTIR spectrum also proves the existence of boehmite within the ruby host. Another mineral species of hydro-aluminum oxide found in corundum is boehmite.

5.4.3. Growth Structures

Sharp and straight growth lines in a hexagonal pattern were usually observed in the majority of samples in this study. Within the growth structures, clouds were composed of numerous minute particles and triangular platy rutile (Figure 14). Even though star rubies have been reported from Longido infrequently, the condensed concentration of clouds and growth lines may lay the groundwork for the birth of an asterism effect in the cabochon stone.

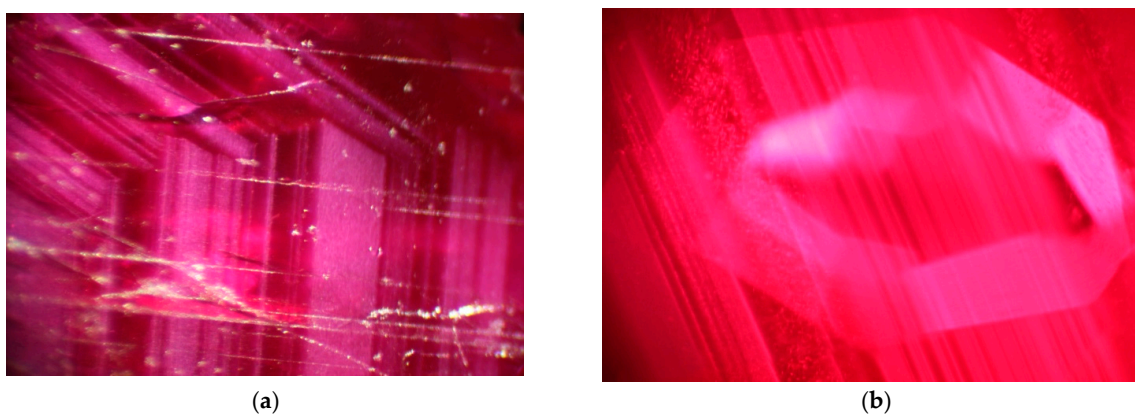


Figure 14. Straight and hexagonal growth structures (a) were commonly observed in these Tanzania rubies, usually accompanied by minute cloudy inclusions and platy rutile (b). Photomicrographs by Yizhi Zhao. Field of widths: (a) 3.04 mm and (b) 6.20 mm.

5.4.4. Fluid Inclusions

Fluid inclusions were found in only a few of the samples studied, as illustrated in Figure 15. These fluids were mainly composed of CO_2 in the healed fractures. The general absence of fluid inclusions may be helpful in contributing to the high clarity and transparency of the material. Meanwhile, the well-formed and untouched shape of the fluids may be a clue to the absence of heat as well.

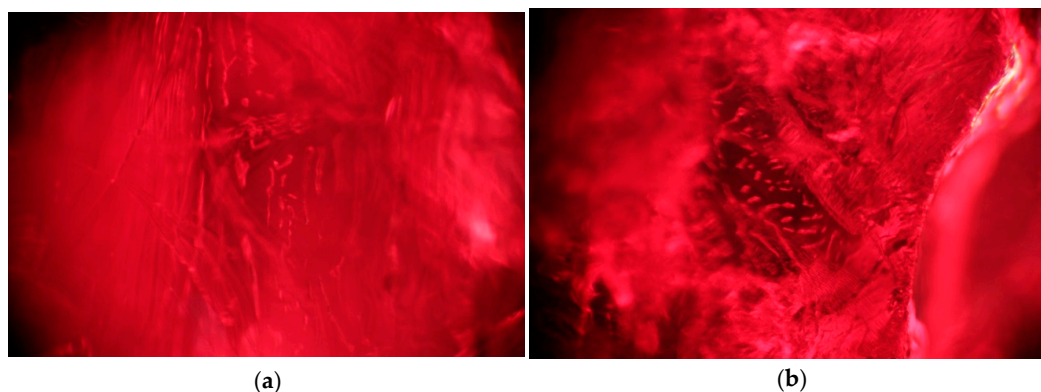


Figure 15. (a,b) Fluid inclusion along the healed fissures was also observed in those Longido rubies. Photomicrographs by Yizhi Zhao. Field of widths: (a) 3.10 mm and (b) 4.10 mm.

5.5. FTIR Spectrum

FTIR tests all the cut stones, and the transmission spectra mainly show peaks around $2000\text{--}3500\text{ cm}^{-1}$. FTIR spectra confirmed the existence of aluminum hydroxide minerals with peaks at 3083 , 2121 , and 1992 cm^{-1} , a common inclusion found in ruby, usually as proof of the absence of heating. The FTIR features of ruby from Longido can be summarized as follows, as illustrated in Figure 16:

- A flat line without any noticeable peak;
- A small peak at 3309 cm^{-1} ;
- Distinct peaks 3311 and 3083 cm^{-1} followed two small peaks at 2121 and 1992 cm^{-1} .

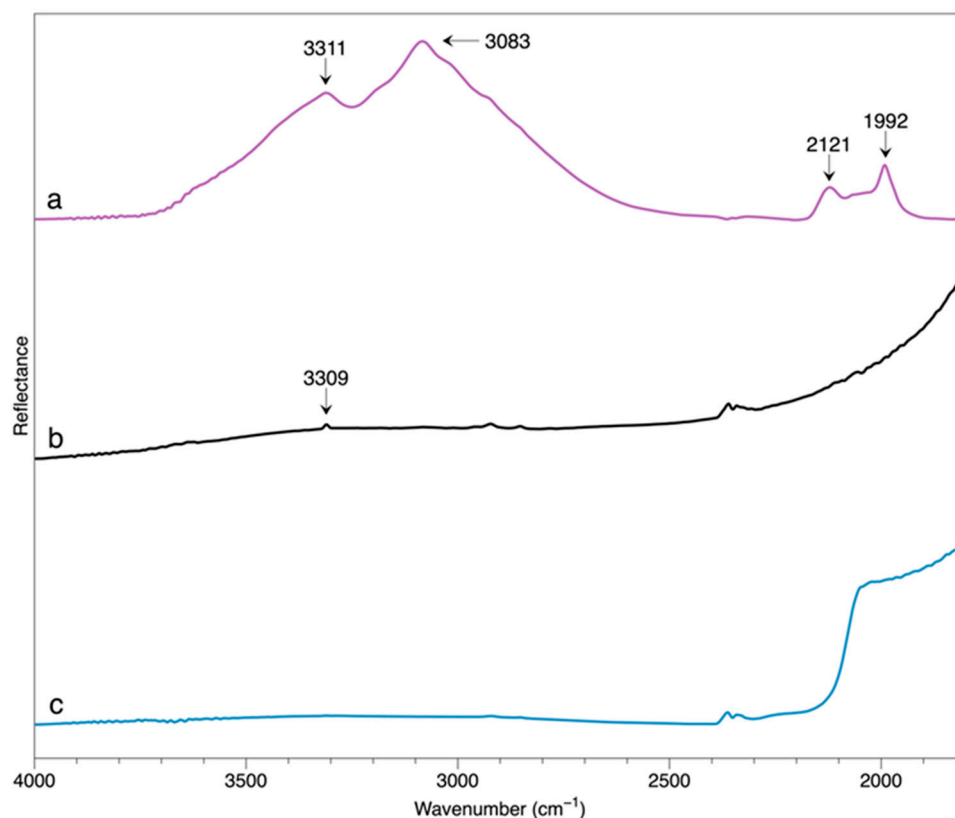


Figure 16. FTIR transmission spectrum shows peaks at 3083 , 2121 , and 1992 cm^{-1} , confirming the existence of aluminum hydroxide minerals.

By comparison, the FTIR spectrum features reported by a previous study of ruby from Winza differ from those of these Longido samples [33]. While the Winza rubies exhibit prominent kaolinite-related peaks at 3695 , 3670 , 3650 , and 3620 cm^{-1} and a distinct peak at 3160 cm^{-1} [33,52], neither of these features has been observed in the ruby from Longido in this study.

5.6. UV-Vis Spectrum

The UV-vis spectrum was carried on the faceted samples, and the polarizer can determine the *c*-axis of the samples. As demonstrated in Figure 17, the UV-Vis-NIR spectroscopy of one ruby sample was collected and oriented in two directions: perpendicular to the *c*-axis ($\perp c$) and parallel to the *c*-axis ($//c$). The Cr^{3+} -related absorption showed bands up to 450 nm , between 520 and 585 nm , and sharp lines at 475 and 694 nm ; faint lines were sometimes seen at 659 and 668 nm . Moreover, a narrow band was observed at 675 nm for the extraordinary ray (e-ray) but not the ordinary ray (o-ray). No prominent Fe-related peaks are present, suggesting a low Fe content level [53].

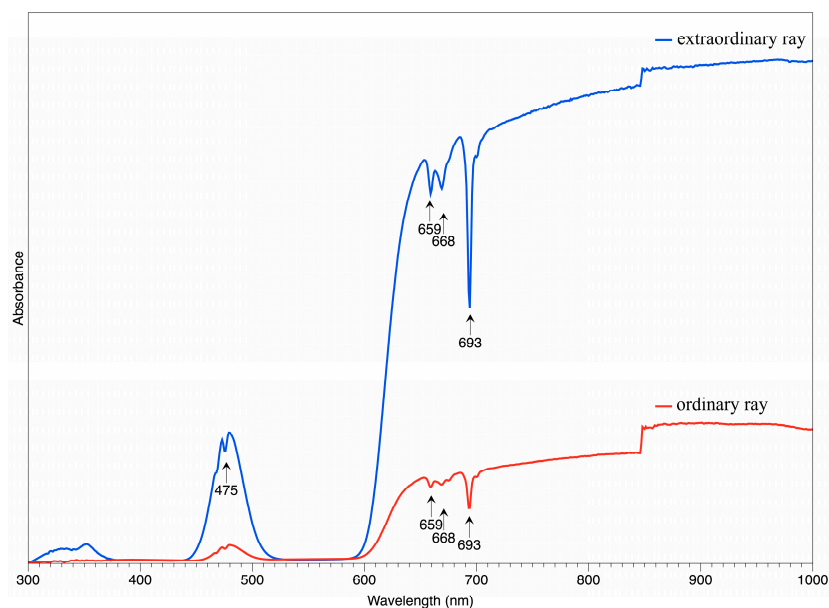


Figure 17. Polarized UV-Vis spectrum of ruby from Longido, Tanzania, showing a broad absorption band centered at 550 nm, with a series of Cr-related peaks at 659, 669, and 694 nm in both ordinary ray (red line) and extraordinary ray (blue line) and one more peak at 675 nm in extraordinary ray.

5.7. Chemical Composition

Elements like Fe, Cr, Ti, Ga, and others may enter the crystalline structure of corundum and take the place of Al as well as be a part of the corundum structure because of their similarities to Al. The diversity and concentration of these replacing cations are closely related to the surrounding environment of corundum. Trace elements may be highly beneficial to distinct rubies from different locales since ruby can develop in a variety of geological environments and occurrences, such as marble in Burma, amphibole in Mozambique, and basalt in Thailand and Cambodia.

The LA-ICP-MS testing revealed the trace elements within the rubies from Longido, Tanzania, as listed in Table 5. The Ti content is at a low level, ranging from 3.64 to 94.54 ppm with an average of 32.14 ppm, and the same situation applies to V, which has a range of 5.58 to 12.47 ppm and an average value as low as 8.83 ppm. Cr is very prominent, starting at 6319 ppm and reaching a peak value of 17,957.6 ppm, while Fe is at a medium to a low level compared with others, falling in the range of 1014.34 to 2817.72 ppm, averaging at 1711.89 ppm. The Longido ruby is poor in Ga, with an average value of 28.55 ppm.

Table 5. The main trace elements of rubies from Longido, Tanzania, in this study, tested by LA-ICP-MS.

Trace Element	Ti	V	Cr	Fe	Ga
Range (ppm)	3.64–94.54	5.58–12.47	6319.47–17,057.60	1014.34–2817.72	23.48–37.51
X (ppm) ^a	32.14	8.83	9962.72	1711.89	28.55
S (ppm) ^b	15.69	1.68	1983.57	355.08	3.66
CV ^c	48.82%	19.06%	19.91%	20.74%	12.81%

^a X = average. ^b S = standard deviation. ^c CV = coefficient of variation.

Furthermore, the values of the coefficients of variation of these five elements also suggest the element distribution uniformity of the ruby. As V, Cr, Fe, and Ga fluctuate at low levels, giving a CV value between 12.81% and 20.74, the Ti is distributed very unevenly in the ruby host and has a CV value of 48.82%. Such big differences in the CV value imply that the distribution behavior of the trace elements within ruby hosts differs from one to another. Caution is advised when using insufficient data to analyze and make a statement when the elemental distribution fluctuates tremendously.

6. Discussion

6.1. Rutile

Rutile is a type of titanium oxide mineral that can be found in rubies of various origins, and they may exhibit different shapes and various combinations, which could serve as a way to facilitate origin determination. For example, rutile in Burmese ruby generally shows short needles, and they are usually concentrated in a condensed way, causing a somehow cloudy appearance (Figure 18). The abundant rutile needles, with proper orientation, may give rise to asterism, and Burma is well-known for producing high-quality star rubies. By comparison, the Mozambique ruby contains rutile that is usually coarse and concentrated relatively sparsely (Figure 19), which also helps explain why asterism is less common in the Mozambique ruby. As shown in Figure 20, the short prismatic form and triangle platy of rutile can be a hallmark of the Longido origin because they are not as long as those found in Mozambique and can be slightly larger than those found in Burmese rubies.

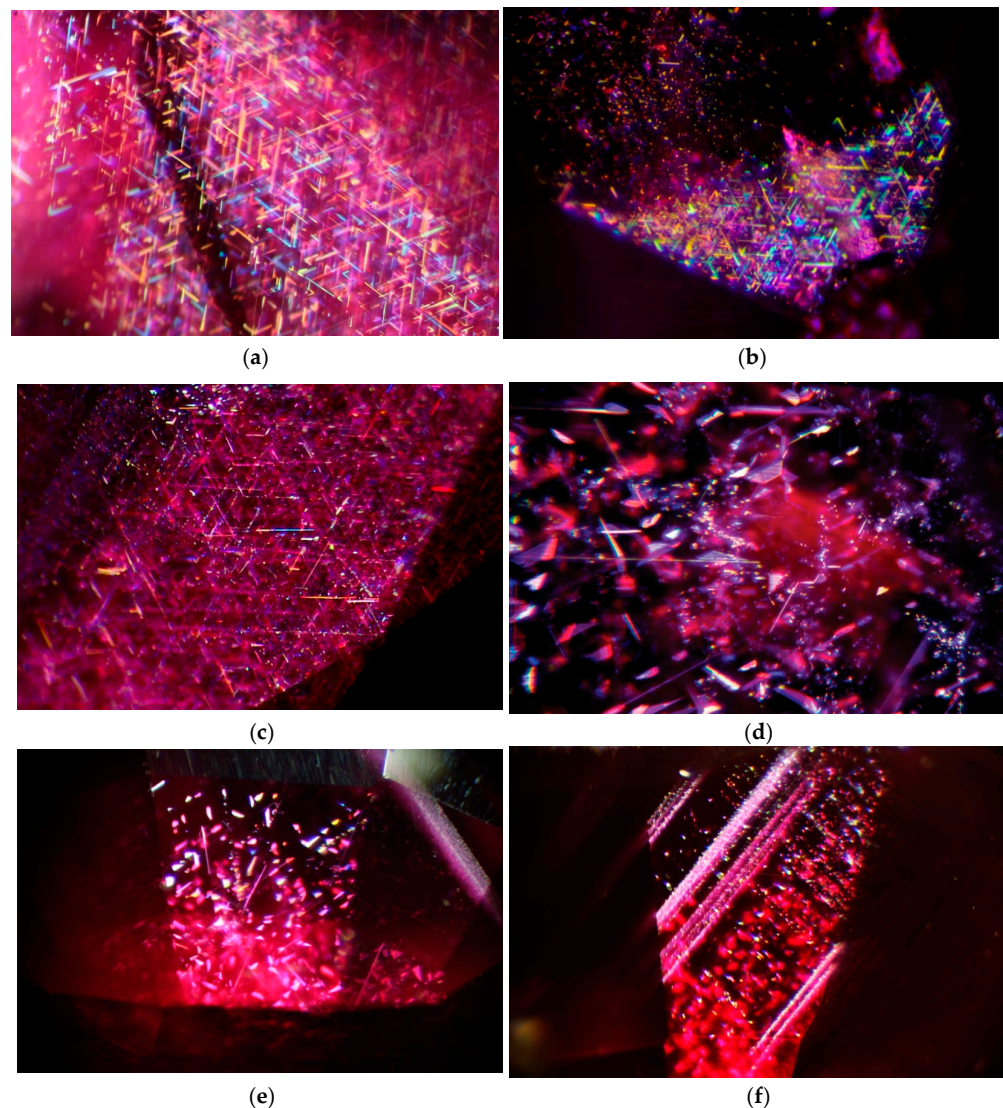


Figure 18. (a,b) Sharp and short needles, aligned with the structure of their ruby host, are classic internal features of unheated rubies from Mogok, Burma. Field of widths: (a) 1.12 mm and (b) 3.66 mm. (c) Iridescent rutile needles in a densely zoned cloud paint a classic portrait of the interior of a natural Mozambique ruby. Field of width: 2.20 mm. (d) Platy and acicular inclusions shine when illuminated with oblique fiber optic light in a natural Mozambique ruby. Field of width: 0.66 mm. (e,f) In this study, rutile was found in ruby from Longido, Tanzania, with a short triangle platy shape. Field of widths: (e) 3.10 mm and (f) 3.43 mm. Photomicrographs by Yizhi Zhao.

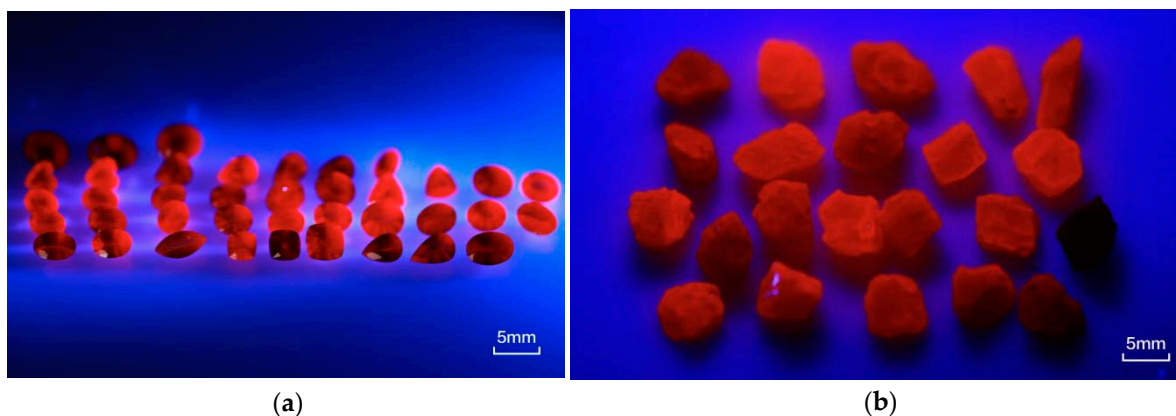


Figure 19. (a,b) Both the faceted rubies and rough from Tanzania showed medium to strong red fluorescence under long wave U.V. light (365 nm). Photos by Yizhi Zhao.

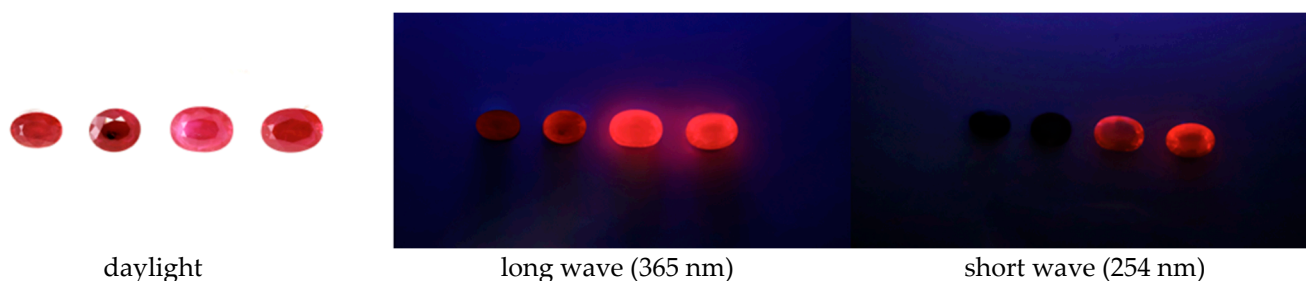


Figure 20. Four rubies from different origins, from left to right: Mozambique, Tanzania, Burma, Synthetic. The light source of each figure: left: daylight, middle: long wave (365 nm), right: short wave (254 nm). Photos by Xueying Sun.

6.2. Fluorescence

Fluorescence is an important gemological property of gemstones, especially in rubies. Because of the Cr content, ruby may exhibit red fluorescence with varying saturations and strengths. Iron is believed to prohibit such behavior. All the rubies, both faceted and rough, showed moderate to strong red fluorescence under a long-wave UV (Figure 19), while being nearly inert to weakly red under a short-wave UV. As a comparison, rubies from Mozambique and Burma were observed, as well as synthetic counterparts grown by the flame fusion method.

When these rubies are exposed to invisible ultraviolet (U.V.) rays, they all exhibit even fluorescence in both long-wave and short-wave U.V., and the color seen is red. In all cases, the strength of these rubies' reactions to long-wave UV was stronger than that to short-wave UV (Figure 20). Four rubies from different origins (from left to right: Mozambique, Tanzania, Burma, Synthetic) displayed various strength of red fluorescence. The U.V. imaging revealed a different fluorescent appearance of these samples, which showed that the intensity of rubies of Burmese origin and synthetic ones was distinctly stronger. In contrast, African ruby presented a much weaker fluorescence, and Mozambique ruby appeared to have the faintest fluorescence.

From the EDXRF data, as listed in Table 6, the Fe concentration was considered to explain the different fluorescent appearances of these samples. Mozambique ruby is enriched in Fe, which will suppress the luminous intensity. Rubies from Burma and synthetic ones are characterized by an extremely low amount of Fe, which may induce a strong reaction under UV rays. Longido ruby, on the other hand, has the highest Cr content (around 8300 ppm) and the intermediate Fe content (around 1200 ppm), resulting in a moderate fluorescence intensity. The Cr/Fe ratios were further proposed, which are presented in Table 6, to explore the relationship between element concentration and fluorescence. It was indicated that the sample with the lowest Cr/Fe ratio, which was

down to around 0.2, showed the faintest fluorescence in this experiment, as illustrated in Figure 21.

Table 6. The Fe and Cr contents (ppmw) of ruby from various sources tested by EDXRF, including Longido, Tanzania, Mozambique, Burma, and Flame fusion method.

Test Point Number	Origin	Fe	Cr	Cr/Fe
Moz-1	Mozambique	5330	1077	0.2
Moz-2	Mozambique	5246	1056	0.2
Moz-3	Mozambique	4997	974	0.19
On Average		5191	1036	0.2
Tan-1	Longido, Tanzania	1278	8588	6.72
Tan-2	Longido, Tanzania	1252	8361	6.68
Tan-3	Longido, Tanzania	1262	8308	6.58
On Average		1264	8419	6.66
Bur-1	Mogok, Burma	49	1643	33.33
Bur-2	Mogok, Burma	52	2547	49.08
Bur-1	Mogok, Burma	51	2578	50.16
On Average		51	2256	44.35
Syn-1	Flame Grown method	42	3233	77.72
Syn-1	Flame Grown method	46	3271	70.95
Syn-1	Flame Grown method	38	3197	85.25
On Average		42	3234	77.48

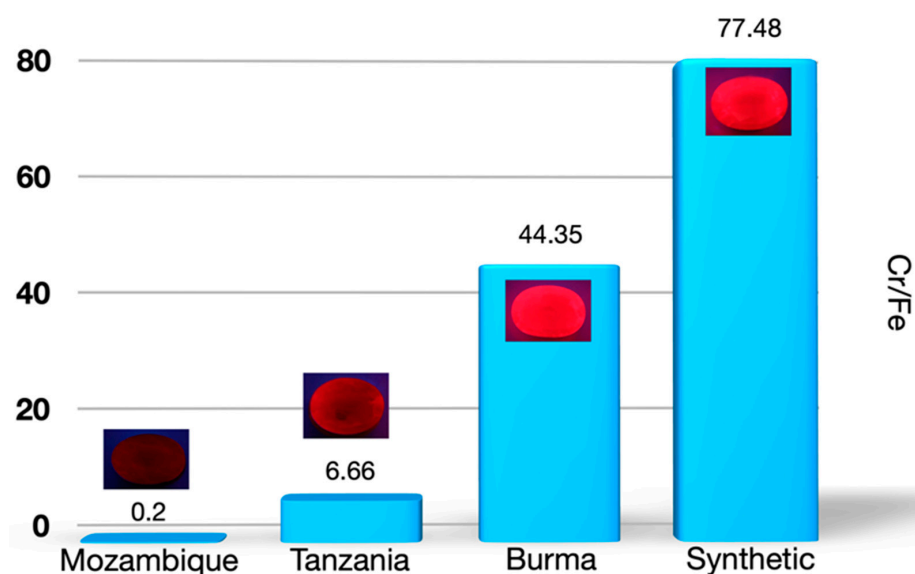


Figure 21. The fluorescence intensity of ruby from various origins may be attributed to the Cr/Fe ratio; the higher Cr/Fe, the stronger fluorescence. Illustrated by Yujie Gao.

In conclusion, the different amounts of Cr and Fe and the Cr/Fe ratio enable us to explain the different fluorescent appearances of rubies, and they can further help discriminate rubies from various sources with different Cr and Fe contents to a degree.

6.3. Trace Elements

The trace elements have been proven to be a powerful tool to determine the origin of ruby, especially when the stones are very clean and their visual appearance shows very little difference [30]. Several elements could be useful, including V, Cr, Ga, Ti, and Fe. As mentioned above, the similarities between these elements and Al allow them to enter the crystalline structure of corundum. However, the ambient environment where ruby is formed may contain these elements at different levels. Hence, the trace element contents and their relative ratio can be an indicator for origin determination. Taking

Burmese, Mozambique, and Longido rubies, for example, the Fe and Cr content can clearly differentiate these three origins (Figure 22). The Fe-free marble-hosted ruby from Burma can be clearly separated from the other two. However, several overlaps still exist between Longido and Mozambique since they both belong to the African continent and are influenced by similar geology events and substance supplies.

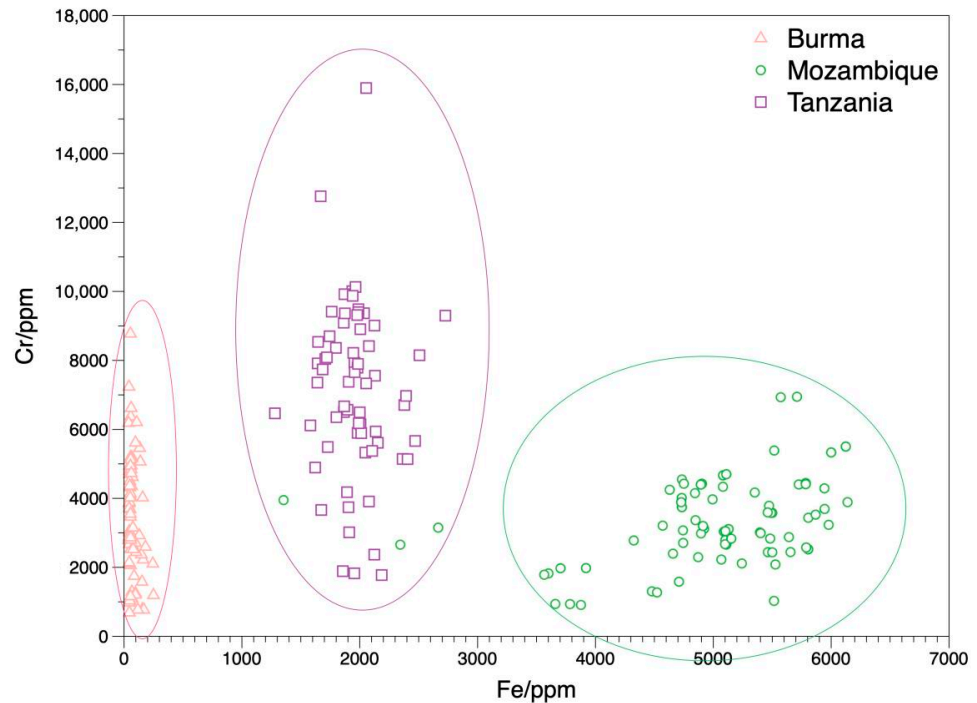


Figure 22. Plotting of Fe and Cr to show the difference in rubies from Mozambique, Burma, and Longido Tanzania in this study.

Furthermore, the extremely high Cr content not only gives rise to the attractive color, of which most can reach the criteria of “Pigeon’s Blood”, as known in the gem trade. Meanwhile, the oversaturation of Cr absorbs too much of the visible light and prohibits reflecting more light back, resulting in more extinction and dark tone in the finished cut stone. Such features prohibit the stone from cutting into large sizes with nice colors of bright tones. As shown in Figure 23, the three-carat stone on the left shows deep red, while the one-carat-size stone exhibits vivid red by contrast.



Figure 23. Two faceted rubies from Longido are compared with different sizes. The high chromium content may prohibit the stone from reflecting more light back, resulting in more extinction and lower tone, especially when the stone is cut into a big size. Photo by Yizhi Zhao.

7. Conclusions

Rubies from Longido, Tanzania, are found with wall rock composed mainly of feldspar, mica, zoisite, and amphibole. The high transparency and clarity enable the stones to be faceted instead of carved or cut as cabochons. The presence of boehmite may be a strong proof of the absence of heating. High chromium and low iron make the color more saturated in red, which is a useful parameter to differentiate them from Burmese and Mozambique rubies. Ongoing studies of the new Mozambique ruby production by FURA Gems, which exhibits high fluorescence, will aim to elucidate the chemical composition of the material in comparison to rubies from Tanzanian and other African ruby sources, including pre-existing ones in Mozambique.

Tanzania is well known for producing high-quality rubies in Winza. Now that Winza is not as active as before, the new production of ruby from the Longido area may further enhance the Tanzanian market share (Figure 24). The relatively large production allows the cutters to perform more interesting and new cutting styles and shapes, giving designers more options. The new production may provide better-quality material for jewelry, especially for small-size rubies. However, the sustainability and stability of supply are still unknown and remain to be seen. Historically, the predominant quality of Longido material has been suitable for carving and for cutting as cabochons. With regard to the material from the pocket productions of 2017 and 2018, a small portion of high-quality facet-grade material has been seen in the market. While those productions have created a lot of interest and investment, the mining for facet-grade material in the hard rock in Longido is much more difficult than the alluvial mining in Mozambique.



Figure 24. Two high-quality rubies from Tanzania: the left one weighs 2.60 ct (from Winza), and the right one weighs 1.07 ct (from Longido). Photo by Yizhi Zhao. Courtesy of Mr. Kenny Yi from Xiangtian Jewelry Ltd. Co. (Shanghai, China).

Author Contributions: Conceptualization, K.L.; Data curation, X.S., T.H. and Y.Z.; Formal analysis, Y.G. and A.C.L.; Funding acquisition, M.H.; Investigation, D.Z. and K.L.; Methodology, Y.G., A.C.L., X.S. and M.L.; Project administration, M.H.; Resources, Y.G.; Software, Y.G., X.S., T.H. and D.F.; Supervision, Y.G., M.H. and D.F.; Validation, D.Z. and X.J.; Visualization, X.S.; Writing—original draft, Y.G.; Writing—review and editing, Y.G., A.C.L., X.S. and M.L. All authors have read and agreed to the published version of the manuscript.

Funding: This research was funded by the National Science and Technology Infrastructure—The National Infrastructure of Mineral, Rock and Fossil Resources for Science and Technology (<http://www.nimrf.net.cn>, accessed on 25 December 2021), and the Program of the Data Integration and Standardization in the Geological Science and Technology from MOST, China, grant number 2013FY110900-3.

Data Availability Statement: The original contributions presented in the study are included in the article, further inquiries can be directed to the corresponding author.

Acknowledgments: Chengsi Wang and Yungui Liu, from China University of Geoscience (Wuhan) are thanked for their help during the Raman and LA-ICP-MS testing. Kenny Yi from Xiangtian Jewelry in Shenzhen is thanked for sharing his seasoned experience in the gem trade. Yizhi Zhao is also thanked for the photography.

Conflicts of Interest: The authors declare no conflicts of interest.

References

1. Shor, R. Auction Houses: A Powerful Market Influence on Major Diamonds and Colored Gemstones. *Gems Gemol.* **2013**, *49*, 2–15. [[CrossRef](#)]
2. Garnier, V.; Giuliani, G.; Ohnenstetter, D.; Fallick, A.E.; Dubessy, J.; Banks, D.; Vinh, H.Q.; Lhomme, T.; Maluski, H.; Pecher, A.; et al. Marble-hosted ruby deposits from Central and Southeast Asia: Towards a new genetic model. *Ore Geol. Rev.* **2008**, *34*, 169–191. [[CrossRef](#)]
3. Giuliani, G.; Ohnenstetter, D.; Fallick, A.E.; Groat, L.; Fagan, J. The geology and genesis of gem corundum deposits. In *Geology of Gem Deposits*, 2nd ed.; Groat, L.A., Ed.; Short Course Series; Mineralogical Association of Canada: Québec, QC, Canada, 2014; Volume 44, pp. 29–112.
4. Garnier, V.; Maluski, H.; Giuliani, G.; Ohnenstetter, D.; Schwarz, D. Ar-Ar and U-Pb ages of marble-hosted ruby deposits from central and southeast Asia. *Can. J. Earth Sci.* **2003**, *43*, 509–532. [[CrossRef](#)]
5. Zaw, K.; Sutherland, L.; Yui, T.F.; Meffre, S.; Thu, K. Vanadium-rich ruby and sapphire within Mogok Gemfield, Myanmar: Implications for gem color and genesis. *Miner. Depos.* **2014**, *50*, 25–39. [[CrossRef](#)]
6. Searle, M.P.; Morley, C.K.; Waters, D.J.; Gardiner, N.J.; Htun, U.K.; Nu, T.T.; Robb, L. Chapter 12 Tectonic and metamorphic evolution of the Mogok Metamorphic and Jade Mines belts and ophiolitic terranes of Burma (Myanmar). *Geol. Soc. Lond. Mem.* **2017**, *48*, 261–293. [[CrossRef](#)]
7. Peretti, A.; Schmetzer, K.; Bernhardt, H.J.; Mouawad, F. Rubies from Mong Hsu. *Gems Gemol.* **1995**, *31*, 2–26.
8. Long, P.V.; Vinh, H.Q.; Nghia, N.X. Inclusions in Vietnamese Quy Chau ruby and their origin. *Aust. Gemmol.* **2004**, *22*, 67–71.
9. Long, P.V.; Vinh, H.Q.; Garnier, V.; Giuliani, G.; Ohnenstetter, D. Marble-hosted ruby from Vietnam. *Can. Gemmol.* **2004**, *25*, 83–95.
10. Long, P.V.; Vinh, H.Q.; Garnier, V.; Giuliani, G.; Ohnenstetter, D.; Lhomme, T.; Schwarz, D.; Fallick, A.; Dubessy, J.; Trinh, P.T. Gem corundum deposits in Vietnam. *J. Gemmol.* **2004**, *29*, 129–147. [[CrossRef](#)]
11. Huang, W.; Ni, P.; Shui, T.; Pan, J.; Fan, M.; Yang, Y.; Chi, Z.; Ding, J. Trace Element Geochemistry and Mineral Inclusions Constraints on the Petrogenesis of a Marble-Hosted Ruby Deposit in Yunnan Province, China. *Can. Mineral.* **2021**, *59*, 381–408. [[CrossRef](#)]
12. Huang, W.; Ni, P.; Zhou, J.; Shui, T.; Ding, J.; Zhu, R.; Cai, Y.; Fan, M. Discovery of Disulfane (H₂S₂) in Fluid Inclusions in Rubies from Yuanjiang, China, and Its Implications. *Crystals* **2021**, *11*, 1305. [[CrossRef](#)]
13. Levinson, A.A.; Cook, F.A. Gem Corundum in Alkali Basalt: Origin and Occurrence. *Gems Gemol.* **1994**, *30*, 253–262.
14. Lin Sutherland, F.; Hoskin, P.W.O.; Fanning, C.M.; Coenraads, R.R. Models of corundum origin from alkali basaltic terrains: A reappraisal. *Contrib. Mineral. Petrol.* **1998**, *133*, 356–372. [[CrossRef](#)]
15. Sutherland, F.L.; Coenraads, R.R. An unusual ruby-sapphire-sapphirine-spinel assemblage from the Tertiary Barrington Volcanic province, New South Wales, Australia. *Mineral. Mag.* **1996**, *60*, 623–638. [[CrossRef](#)]
16. Yui, T.F.; Zaw, K.; Limtrakun, P. Oxygen isotope composition of the Denchai sapphire, Thailand: A clue to its enigmatic origin. *Lithos* **2003**, *67*, 153–161. [[CrossRef](#)]
17. Saminpanya, S.; Sutherland, F.L. Different origins of Thai area sapphire and ruby, derived from mineral inclusions and co-existing minerals. *Eur. J. Mineral.* **2011**, *23*, 683–694. [[CrossRef](#)]
18. Palke, A.C.; Wong, J.; Verdel, C.; Avila, J.N. A common origin for Thai/Cambodian rubies and blue and violet sapphires from Yogo Gulch, Montana, U.S.A.? *Am. Mineral.* **2018**, *103*, 469–479. [[CrossRef](#)]
19. Chapin, M.; Pardieu, V.; Lucas, A. Mozambique: A Ruby Discovery for the 21st Century. *Gems Gemol.* **2015**, *51*, 44–54.

20. Sorokina, E.S.; Rösel, D.; Häger, T.; Mertz-Kraus, R.; Saul, J.M. LA-ICP-MS U–Pb dating of rutile inclusions within corundum (ruby and sapphire): New constraints on the formation of corundum deposits along the Mozambique belt. *Miner. Depos.* **2017**, *52*, 641–649. [[CrossRef](#)]
21. Vertriest, W.; Saeseaw, S. A Decade of Ruby from Mozambique: A Review. *Gems Gemol.* **2019**, *55*, 162–183. [[CrossRef](#)]
22. Mercier, A.; Rakotondrazafy, M.; Ravolomiandrinarivo, B. Ruby mineralization in southwest Madagascar. *Gondwana Res.* **1999**, *2*, 433–438. [[CrossRef](#)]
23. Cartier, L.E. Ruby and sapphire from Marosely, Madagascar. *J. Gemmol.* **2009**, *31*, 171–179. [[CrossRef](#)]
24. Goff, E.L.; Deschamps, Y.; Guerrot, C. Tectonic implications of new single zircon Pb–Pb evaporation data in the Lossogonoi and Longido ruby-districts, Mozambican metamorphic Belt of north-eastern Tanzania. *C. R. Geosci.* **2010**, *342*, 36–45. [[CrossRef](#)]
25. Smith, C.P.; Fagan, A.J.; Clark, B. Ruby and Pink Sapphire from Aappaluttoq, Greenland. *J. Gemmol.* **2016**, *35*, 294–306. [[CrossRef](#)]
26. Yakymchuk, C.; Szilas, K. Corundum formation by metasomatic reactions in Archean metapelite, SW Greenland: Exploration vectors for ruby deposits within high-grade greenstone belts. *Geosci. Front.* **2018**, *9*, 727–749. [[CrossRef](#)]
27. Keulen, N.; Thomsen, T.B.; Schumacher, J.C.; Poulsen, M.D.; Kalvig, P.; Vennemann, T.; Salimi, R. Formation, origin, and geographic typing of corundum (ruby and pink sapphire) from the Fiskebøl complex, Greenland. *Lithos* **2020**, *366*, 105536. [[CrossRef](#)]
28. Pignatelli, I.; Morlot, C.; Giuliani, G.; Pardieu, V. The ‘Star of David’ Pattern and Presence of Macro-steps on Ruby and Sapphire Crystals from Aappaluttoq, Greenland. *J. Gemmol.* **2022**, *38*, 364–375. [[CrossRef](#)]
29. Giuliani, G.; Groat, L.A. Geology of Corundum and Emerald Gem Deposits: A Review. *Gems Gemol.* **2019**, *55*, 464–489. [[CrossRef](#)]
30. Palke, A.C.; Saeseaw, S.; Renfro, N.D.; Sun, Z.; McClure, S.F. Geographic Origin Determination of Ruby. *Gems Gemol.* **2019**, *55*, 480–613. [[CrossRef](#)]
31. Dirlam, D.M.; Misorowski, E.B.; Tozer, R.; Stark, K.B.; Bassett, A.M. Gem wealth of Tanzania. *Gems Gemol.* **1992**, *28*, 80–102.
32. Hanni, H.A.; Schmetzer, K. New rubies from the Morogoro area, Tanzania. *Gems Gemol.* **1991**, *27*, 156–167.
33. Schwarz, D.; Pardieu, V.; Saul, J.; Schmetzer, K.; Laurs, B.; Giuliani, G.; Klemm, L.; Malsy, A.; Erel, E.; Hauzenberger, C.; et al. Rubies and Sapphires from Winza, Central Tanzania. *Gems Gemol.* **2008**, *44*, 322–347. [[CrossRef](#)]
34. Hanni, H. On corundum from Uмба Valley, Tanzania. *J. Gemmol.* **1987**, *20*, 278–284. [[CrossRef](#)]
35. Chankhantha, C.; Kidkhunthod, P.; Amphon, R.; Shen, A.H. Gemological and XANES Investigations Of Pink Spinel From Mahenge, Tanzania. In Proceedings of the 3rd International Conference on Radiation and Emission in Materials (ICREM), Chiang Mai, Thailand, 15–18 December 2020.
36. Chankhantha, C.; Amphon, R.; Rehman, H.; Shen, A. Characterisation of Pink-to-Red Spinel from Four Important Localities. *J. Gemmol.* **2020**, *37*, 393–403. [[CrossRef](#)]
37. Feneyrol, J.; Giuliani, G.; Demaiffe, D.; Ohnenstetter, D.; Fallick, A.E.; Dubessy, J.; Martelat, J.; Rakotondrazafy, A.F.; Omito, E.; Ichangi, D.; et al. Age and Origin of the Tsavorite and Tanzanite Mineralizing Fluids in the Neoproterozoic Mozambique Metamorphic Belt. *Can. Mineral.* **2017**, *55*, 763–786. [[CrossRef](#)]
38. Pohl, W.L. The Tsavorite (Gem Quality Vanadium Grossularite) Minerogenetic System in East Africa. In *The Structural Geology Contribution to the Africa-Eurasia Geology: Basement and Reservoir Structure, Ore Mineralization and Tectonic Modelling. CAJG 2018. Advances in Science, Technology & Innovation*; Springer: Cham, Switzerland, 2019.
39. Schmetzer, K.; Malsy, A.-K. Alexandrite and color-change chrysoberyl from the Lake Manyara alexandrite-emerald deposit in northern Tanzania. *J. Gemmol.* **2011**, *32*, 179–209. [[CrossRef](#)]
40. Leelawatanasuk, T.; Susawee, N.; Bupparenoo, P. Characteristics of Faceted-Quality Ruby from Longido, Tanzania. *Bull. Earth Sci. Thail.* **2021**, *10*, 1–7.
41. Kongsomart, B.; Vertriest, W.; Weeramankhonlert, V. Preliminary Observations on Facet-Grade Ruby from Longido, Tanzania. *Gems Gemol.* **2017**, *53*, 472–473.
42. Sumritvanicha, N.; Sripoonjan, T.; Wanthanachaisaeng, B. Indication of Low-Temperature Heat Treatment: The Case Study of Ruby from Longido, Tanzania. In Proceedings of the 43rd Congress on Science and Technology of Thailand (STT 43), Bangkok, Thailand, 17–19 October 2017.
43. Gao, Y.J.; Lucas, A.; Sun, X.Y.; Ju, D. Gemological Study of Rubies from Longido, Tanzania. In Proceedings of the 2021 International Jewelry Academic Exchange Conference, Guangzhou, China, 19 November 2021; pp. 70–75.
44. Schlüter, T. Geological Atlas of Africa. In *With Notes on Stratigraphy, Tectonics, Economic Geology, Geohazards and Geosites of Each Country*; Springer: Berlin/Heidelberg, Germany, 2006; pp. 226–231.
45. Balmer, W.; Hauzenberger, C.; Fritz, H.; Sutthirat, C. Marble-hosted ruby deposits of the Morogoro Region, Tanzania. *J. Afr. Earth Sci.* **2017**, *134*, 626–643. [[CrossRef](#)]
46. Abduriyim, A.; Kitawaki, H. Applications of Laser Ablation—Inductively Coupled Plasma—Mass Spectrometry (LA-ICP-MS) to Gemology. *Gems Gemol.* **2006**, *42*, 98–118. [[CrossRef](#)]
47. Hu, Z.C.; Gao, S.; Liu, Y.S.; Hu, S.H.; Chen, H.H.; Yuan, H.L. Signal enhancement in laser ablation ICP-MS by addition of nitrogen in the central channel gas. *J. Anal. At. Spectrom.* **2008**, *23*, 1093–1101. [[CrossRef](#)]
48. Liu, Y.S.; Hu, Z.C.; Gao, S.; Gunther, D.; Xu, J.; Gao, C.G.; Chen, H.H. In situ analysis of major and trace elements of anhydrous minerals by LA-ICP-MS without applying an internal standard. *Chem. Geol.* **2008**, *257*, 34–43. [[CrossRef](#)]

49. Liu, Y.S.; Gao, S.; Hu, Z.C.; Gao, C.G.; Zong, K.Q.; Wang, D.B. Continental and oceanic crust recycling-induced melt-peridotite interactions in the Trans-North China orogen: U/Pb dating, Hf isotopes and trace elements in zircons from mantle xenoliths. *J. Petrol.* **2010**, *51*, 537–571. [[CrossRef](#)]
50. Gao, Y.; Lin, M.; Li, X.; Sun, X. Trace elements and big data application to gemology by x-ray fluorescence. In *Artificial Intelligence and Spectroscopic Techniques for Gemology Applications*; IOP Publishing: Bristol, UK, 2022. [[CrossRef](#)]
51. Anthony, J.W. *Handbook of Mineralogy: Silica, Silicates*; Mineral Data Pub, 1995.
52. Beran, A.; Rossman, G.R. OH in naturally occurring corundum. *Eur. J. Mineral.* **2006**, *18*, 441–447. [[CrossRef](#)]
53. Dubinsky, E.V.; Stone-Sundberg, J.; Emmett, J.L. A Quantitative Description of the Causes of Color in Corundum. *Gems Gemol.* **2020**, *56*, 2–28. [[CrossRef](#)]

Disclaimer/Publisher’s Note: The statements, opinions and data contained in all publications are solely those of the individual author(s) and contributor(s) and not of MDPI and/or the editor(s). MDPI and/or the editor(s) disclaim responsibility for any injury to people or property resulting from any ideas, methods, instructions or products referred to in the content.